Institute for Materials Research, Tohoku University, Sendai[1])

Structure and Magnetic Properties of Fe–Ti–N Films Deposited by DC Magnetron Facing Target Sputtering

By

D. L. Peng, K. Sumiyama, M. Oku, D. X. Li, and K. Suzuki

Using a facing target sputtering equipment, Fe–Ti–N films were deposited on water-cooled and heated substrates under different nitrogen flow ratios, $R(N_2)$. The composition, microstructure, and magnetic properties of the films were investigated by Auger electron spectroscopy (AES), X-ray photoelectron spectroscopy (XPS), X-ray diffraction (XRD), and a vibrating sample magnetometer (VSM). The films consist of α-Fe, TiN_x, and Fe_4N, where the volume fraction of these phases varies with $R(N_2)$ and the substrate temperature during sputtering. The α-Fe(Ti) films with supersaturated nitrogen exhibit a larger M_s than the Fe–Ti films. However, H_c first decreases and then increases with increasing $R(N_2)$. This is ascribed to a distortion of the α-Fe lattice due to doping of Ti atoms and the compressive stress caused by the incorporation of sufficient nitrogen atoms.

1. Introduction

Recently many researches have been devoted to nanocrystalline thin films with high flux density, which are necessary for use in high density magnetic recording heads. In particular, much attention has been focused on Fe–N films, because of their excellent magnetic properties, in combination with the significant improvement of corrosion and wear resistance, compared to pure iron [1 to 7]. Although the Fe–N film has high magnetic flux density, it shows high magnetostriction and poor thermal stability. The addition of third elements to form ternary Fe–M–N films (M = Ta, Zr, Hf, Nb,...) [8 to 12] has succeeded in solving these magnetic and thermal weak points. Microstructure and magnetic properties of ternary Fe–Ti–N films have not been reported yet, in contrast to the systematic works on structure, magnetic properties, and thermal stability of binary Fe–Ti alloy films prepared by vapor quenching [13 to 17]. This paper reports on the structure and magnetic properties of the Fe–Ti–N films produced by dc reactive sputtering at different nitrogen flow ratios $R(N_2)$ and substrate temperatures T_s.

2. Experimental

Fe–Ti–N films were deposited on glass substrates and polyimide substrates by facing-target-type dc magnetron sputtering in a mixed Ar + N_2 plasma, using a composite target consisting of pure Fe (99.9%) and Ti (99.9%) plates. The Fe and Ti concentration ratio was adjusted by changing the ratio of the surface areas of Fe and Ti plates. In

[1]) Katahira 2-1-1, Aoba-Ku, Sendai 980, Japan. E-mail: peng@snap8.imr.tohoku.ac.jp.

Table 1

Sputtering conditions

background pressure (Pa)	$<2 \times 10^{-2}$
total pressure (Pa)	9.3×10^{-1}
nitrogen flow ratio (%)	0 to 35.5
input power (kW)	0.95
magnetic field (kA m^{-1})	
at the target center	8
at the target edge	12
substrate temperature (°C)	$\approx$50, 150, 250, 340
substrate	glass and polyimide
deposition rate (nm s^{-1})	$\approx$1.5

order to obtain Fe–Ti–N films with various nitrogen contents $R(N_2)$ defined as $R(N_2) = [N_2$ flow rate]/[Ar flow rate $+ N_2$ flow rate], was changed by fine control of the mass flowmeters. The substrate temperature during the sputtering deposition was kept at about 50 °C by indirect water cooling and at 150, 250, and 340 °C by indirect resistive heating, respectively. The sputtering conditions are listed in Table 1. The chemical composition of deposited films was determined by inductively coupled plasma (ICP) optical emission spectrometry and helium carrier fusion–thermal conductivity methods.
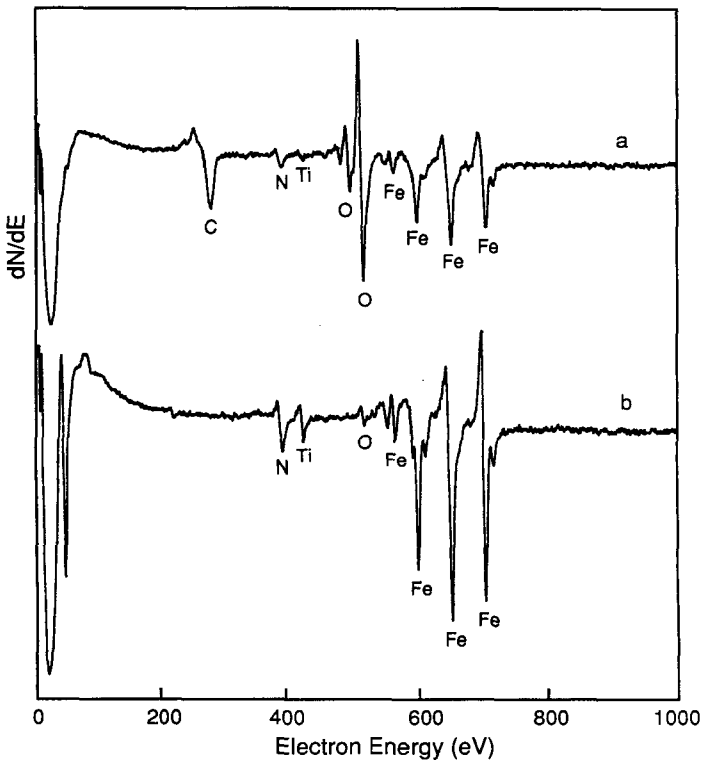

Fig. 1. Typical AES spectra of the Fe–Ti–N films: (a) before sputtering, (b) after sputtering for 3 min

The structures of the films were analysed by X-ray diffraction with CuKα radiation using a graphite monochromator. Auger electron spectroscopy (AES) and X-ray photoelectron spectroscopy (XPS) were done to analyse their chemical compositions and states. The magnetic properties of the films were measured by a vibrating sample magnetometer (VSM) in a magnetic field up to 10 kOe applied parallel and perpendicular to the plane of the films.

3. Results and Discussion

3.1 Composition and structure

Fig. 1 shows typical Auger electron spectra of the Fe–Ti–N films in $Ar + N_2$ mixture with $R(N_2) = 20\%$ on water cooled substrates. Large amounts of oxygen and carbon are observed in the film surface, while the Auger peak intensities of oxygen and carbon disappear almost completely when the film was sputtered with Ar^+ for 3 min. This indicates that the oxygen and carbon in Fig. 1a are mainly due to surface absorption from the ambient atmosphere and oxygen and carbon contamination is very small in the inner parts of these films. Fig. 2 is the AES concentration–depth profile of the same film sample, which shows uniform nitrogen, iron, and titanium contents along the thickness (perpendicular direction) of the film.

Fig. 3 shows the evolution of X-ray diffraction patterns as a function of $R(N_2)$. The (110) peaks shift to a lower 2θ side (the lattice expands) as $R(N_2)$ increases. The peaks show similar 2θ dependences for both alloy films made with target area ratios of Fe:Ti = 7:3 and 8:2. No evidence was found for Fe–N compounds up to $R(N_2) = 30\%$. Below $R(N_2) = 20\%$, Ti atoms apparently dissolve substitutionally and

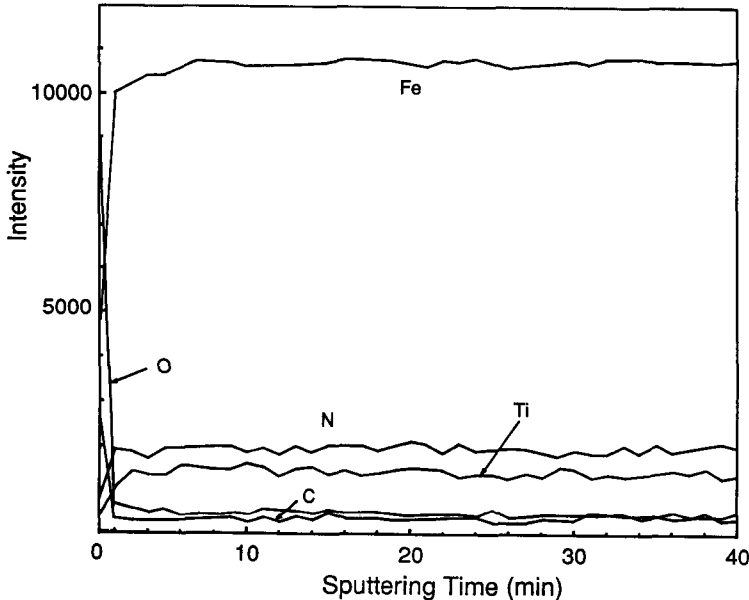
Fig. 2. The AES concentration–depth profiles of the Fe–Ti–N film deposited on water cooled substrates at $R(N_2) = 20\%$
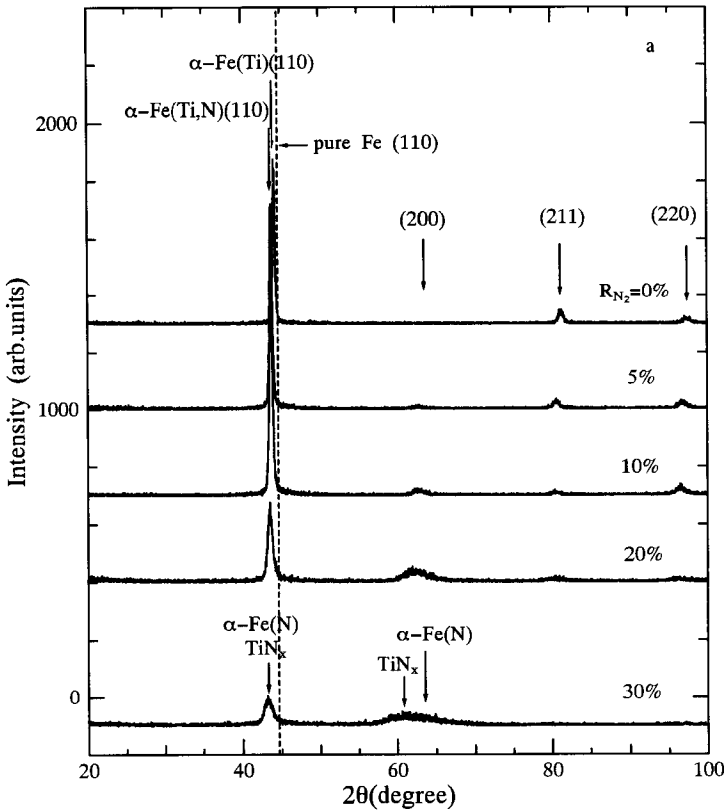
Fig. 3 a

nitrogen atoms interstitially in the b.c.c. Fe lattice. At $R(N_2) = 30\%$, very broad X-ray diffraction peaks obviously indicate formation of a second phase. However, it is difficult to determine phases in the films by conventional X-ray diffraction.

As shown in Fig. 4 and 5, XPS results indicate Fe_{2p}, Ti_{2p}, and N_{1s} XPS peaks of the Fe–Ti and Fe–Ti–N films deposited on water cooled substrates at $R(N_2) = 0$ and 30%. The sample surfaces were cleaned by Ar^+ ion sputtering for 5 min before the XPS measurements. For both Fe–Ti and Fe–Ti–N films, the binding energies of $Fe_{2p_{3/2}}$ and $Fe_{2p_{1/2}}$ are 706.9 and 720.0 eV, being in agreement with those of metallic iron [18]. The binding energies of $Ti_{2p_{3/2}}$ and $Ti_{2p_{1/2}}$ (454.9 and 460.8 eV) in the Fe–Ti–N film are the same to those of TiN_x [18], being different from that of $Ti_{2p_{3/2}}$ and $Ti_{2p_{1/2}}$ (453.9 and 459.8 eV) in the Fe–Ti film. These results indicate that the electronic states of Fe atoms in the Fe–Ti–N film is similar to that of pure metallic iron, and Ti atoms to that of TiN_x. Therefore, the broad peaks of the X-ray diffraction pattern $(R(N_2) = 30\%)$ in Fig. 3 are allotted to the α-Fe and TiN_x phases.

It is worth noting that Fe–N compounds do not appear in the Fe–Ti–N films deposited at $R(N_2) \le 30\%$, where the maximum nitrogen content is about 11.2 at% (from Table 2, corresponding to Fig. 3). Fig. 6 shows X-ray diffraction patterns of the Fe–N and Fe–Ti–N films prepared under the same deposition conditions at different target
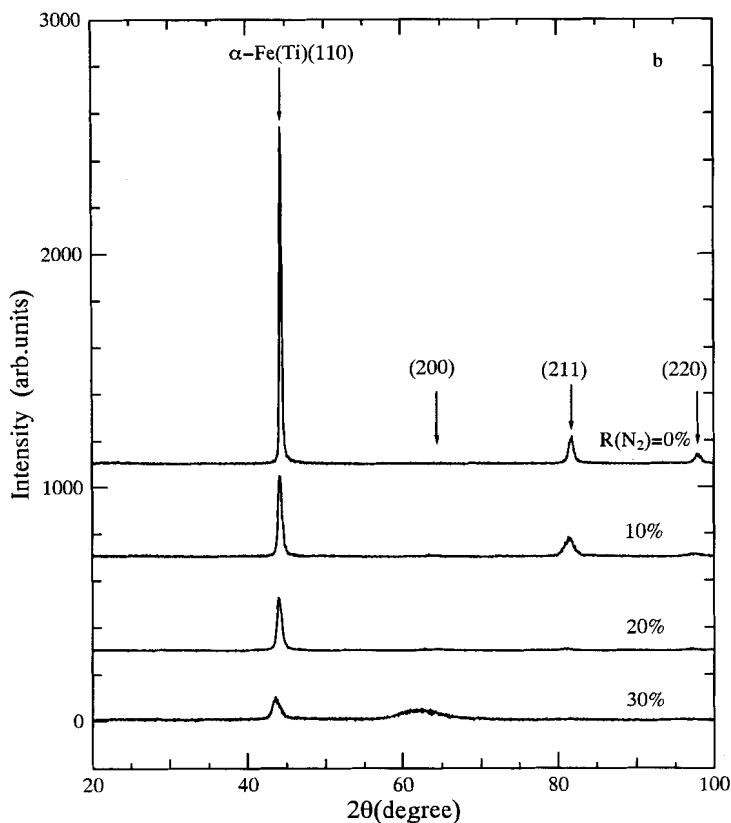
Fig. 3. X-ray diffraction pattern of the Fe–Ti–N films deposited from a composite target with area ratio of a) Fe:Ti = 7:3 and b) 8:2 on water cooled substrates

Table 2

Composition analysis results of the Fe–Ti–N films

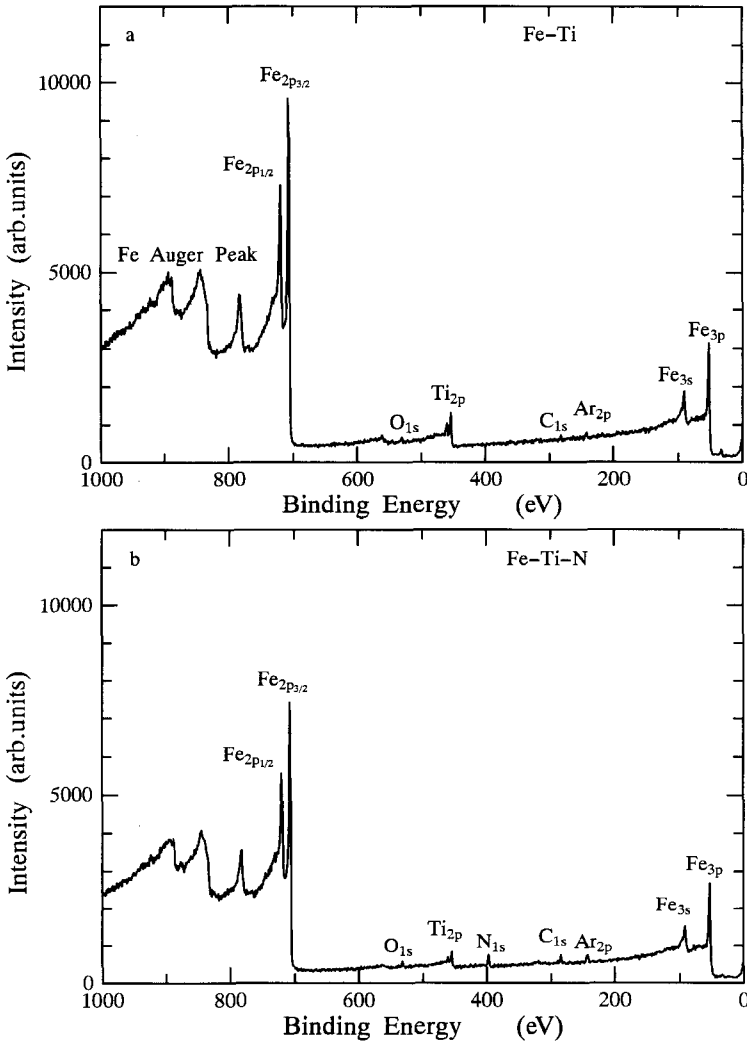| area ratio of target	$R(N_2)$ (%)	Fe (at%)	Ti (at%)	N (at%)
Fe:Ti = 7:3	0	89.7	10.3	
	5	89.0	8.5	2.5
	10	88.6	8.3	3.1
	13.5	88.2	7.5	4.3
	20	87.1	7.0	5.9
	30	83.9	4.9	11.2
Fe:Ti = 8:2	0	94.1	5.9	
	10	93.3	4.9	1.8
	20	92.0	4.4	3.6
	30	85.7	2.7	11.6

Fig. 4. XPS survey spectra for Fe–Ti and Fe–Ti–N films deposited on water cooled substrates at $R(N_2) = 0$ and 30%, respectively

area ratios. The sputter-deposited Fe–N film consists of the α-Fe and γ'-Fe$_4$N phases, while the sputter-deposited Fe–Ti–N film contains the TiN$_x$ phase but no γ'-Fe$_4$N phase. This suggests that Ti atoms react much more preferentially with N in comparison to Fe.

The lattice constant a calculated from the interplanar distance d_{110} of the α-Fe(110) peak is plotted versus $R(N_2)$ in Fig. 7. The values of a of these films are always larger than those of pure Fe and Fe–Ti films and increase with increasing $R(N_2)$. Moreover, the larger the Ti area of Fe–Ti composite target is, the larger is the increase of the lattice constant at the same $R(N_2)$ value. For the target area ratio of Fe:Ti = 7:3, the lattice constant of the α-Fe(7.5 at% Ti–4.3 at% N) film made at $R(N_2) = 13.5\%$ is 2%
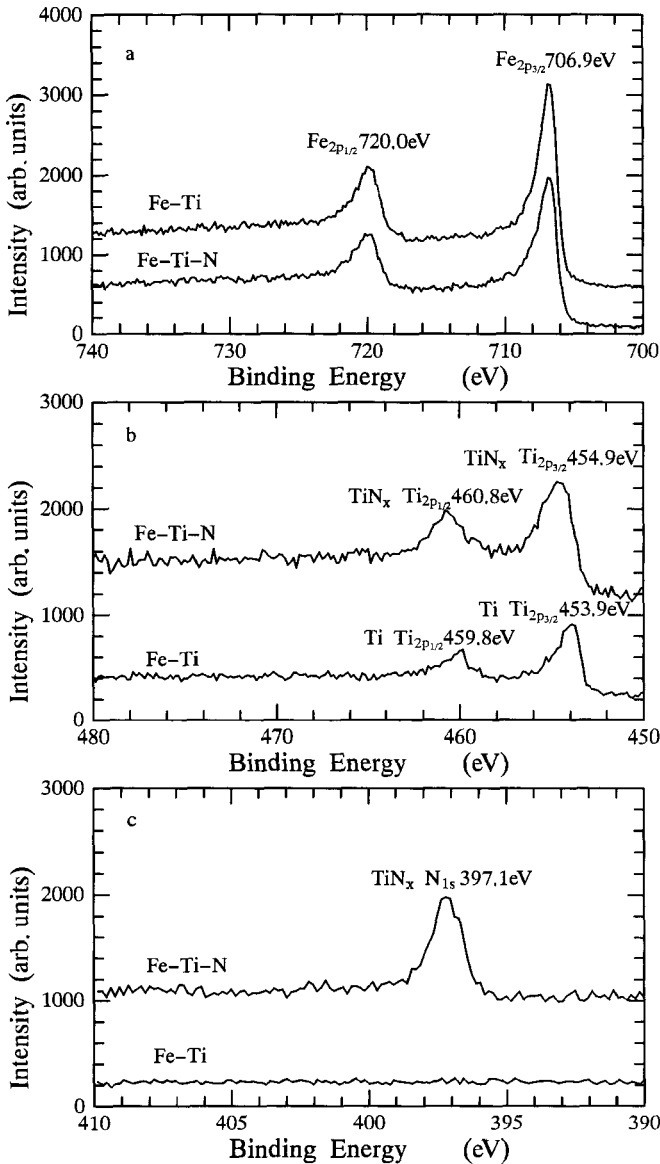
Fig. 5. a) Fe, b) Ti, and c) N peaks in the XPS of the Fe–Ti and Fe–Ti–N films

larger than that of the pure Fe film due to the incorporation of nitrogen atoms, while the lattice constant of the α-Fe–10.3 at% Ti film made at $R(N_2) = 0$ is about 0.9% larger than that of the pure Fe film.

The X-ray diffraction patterns of the Fe–Ti–N films deposited at 250 °C are shown in Fig. 8. It is found that the crystal structure of these films varies from α-Fe to α-Fe $+$ TiN$_x$, and finally α-Fe $+ \gamma'$-Fe$_4$N $+$ TiN$_x$ with the increase in $R(N_2)$. The XRD pattern shows the different preferred orientations of the γ'-Fe$_4$N phase in two films de-
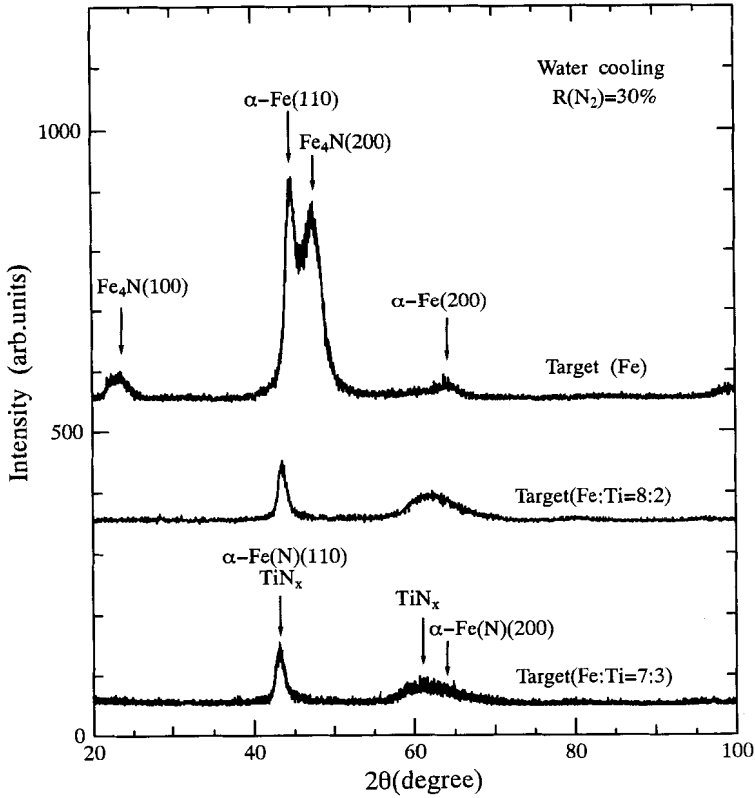
Fig. 6. X-ray diffraction patterns of the Fe–N and Fe–Ti–N films deposited on water cooled substrates at $R(N_2) = 30\%$
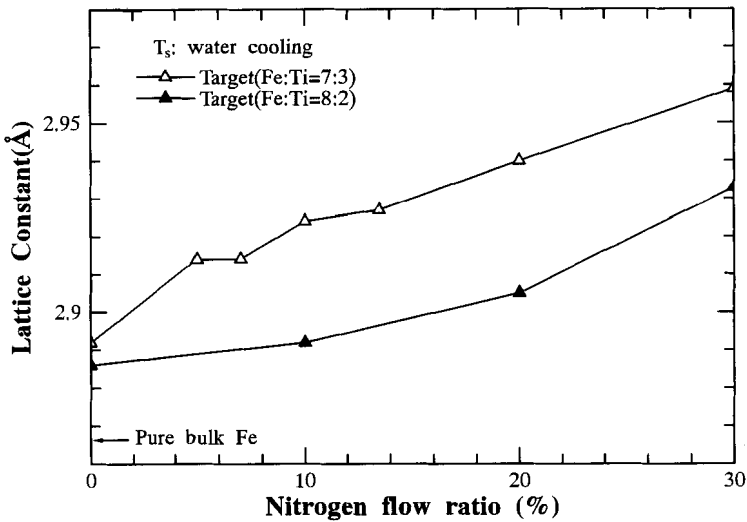

Fig. 7. Lattice constant of b.c.c. Fe–Ti–N films deposited on water cooled substrates
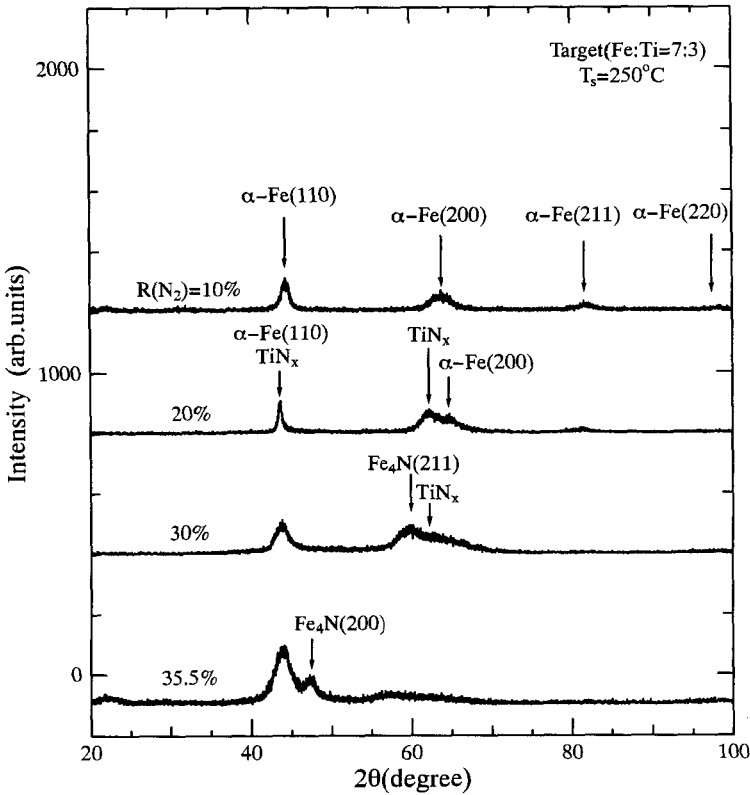
Fig. 8. X-ray diffraction patterns of the Fe–Ti–N films deposited at substrate temperature 250 °C

posited at $R(N_2) = 30$ and 35.5%. Fig. 9 shows the XRD patterns of films deposited at different substrate temperatures at $R(N_2) = 20$%. The change of the crystal structure of these films with increasing T_s is not obvious; these films consist of α-Fe and TiN$_x$ phases.

3.2 Magnetic properties

Fig. 10a and b show the saturation magnetization M_s, coercivity H_c, and the magnetic moment per Fe atom as a function of $R(N_2)$. The M_s value of the film deposited from a pure Fe target on a water cooled substrate is 209 emu/g, but those of the Fe–Ti films deposited from composite targets of Fe:Ti = 7:3 and 8:2 under the same deposition conditions are 176 and 193 emu/g, respectively. The M_s value of the Fe–Ti–N films increases with increasing $R(N_2)$ in both films, as observed in the Fe–N films [6, 7, 19]. The increase in M_s can be ascribed to the expansion of the α-Fe lattice owing to the incorporation of N atoms. Assuming that the Ti and N atoms carry no magnetic moment, we have the $R(N_2)$ dependence of the magnetic moment per Fe atom in the Fe–Ti–N films as shown in Fig. 10b. In accordance with M_s, the magnetic moment of Fe atoms increases with increasing $R(N_2)$. This tendency indicates that the magnetic moment of the Fe atom depends on the number of the nonmagnetic Ti atoms on its
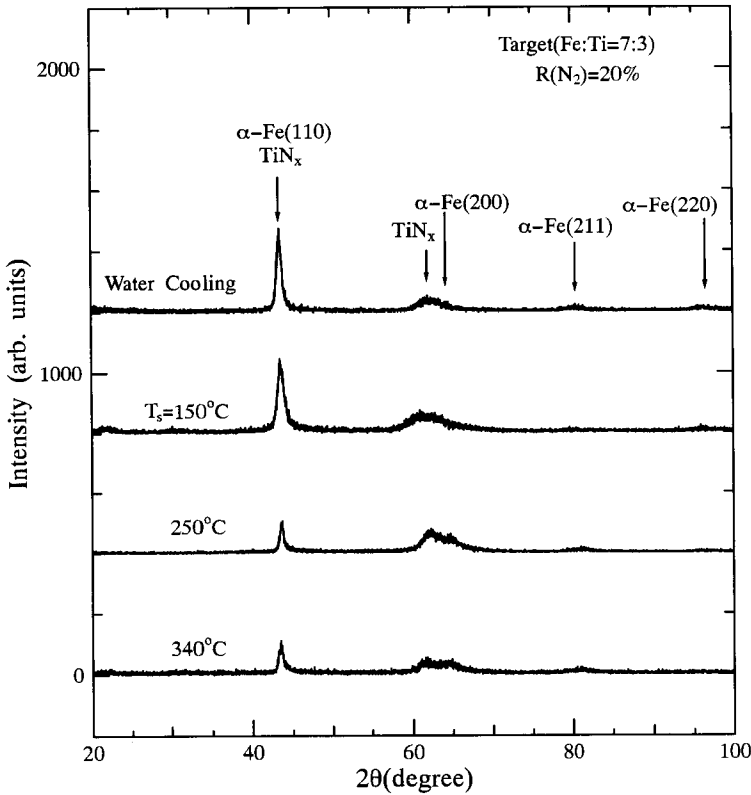
Fig. 9. X-ray diffraction patterns of the Fe–Ti–N films deposited at $R(N_2) = 20\%$ at different substrate temperatures

nearest neighbor atomic sites and N atoms on its neighboring interstitial sites, causing the lattice expansion.

In contrast to the monotonic change in M_s, the $R(N_2)$ dependence of H_c is more complicated. H_c of the films first decreases and then increases with increasing $R(N_2)$. For the Fe–N films, the incorporation of nitrogen atoms results in a compressive stress in the films and causes the increase in H_c [6]. For the Fe–Ti–N films, however, doping of Ti atoms causes the distortion of the α-Fe lattice owing to the different atomic radii of Fe and Ti. In Fig. 10a, H_c decreases at $R(N_2) < 10\%$ owing to the incorporation of nitrogen atoms, causing a slight relaxation of internal stress in the Fe–Ti–N films. H_c increases with further increasing $R(N_2)$ because the incorporation of a large amount of nitrogen atoms results in a compressive stress in the films. An investigation by Takahashi et al. [20] indicated that the soft magnetic properties in Fe–N films are related to the decrease in the total magnetic anisotropy energy in the (110) plane. This is due to the combined effects of tetragonal deformation and grain size reduction.

Fig. 11 shows the change in M_s and H_c as a function of $R(N_2)$ for the films deposited at $T_s = 250\,°C$. M_s of the films increases up to $R(N_2) = 30\%$, in agreement with that of films deposited on water cooled substrates, and then decreases with increasing $R(N_2)$. M_s for α-Fe is larger than that for γ'-Fe$_4$N, the decrease in M_s is ascribed to the forma-
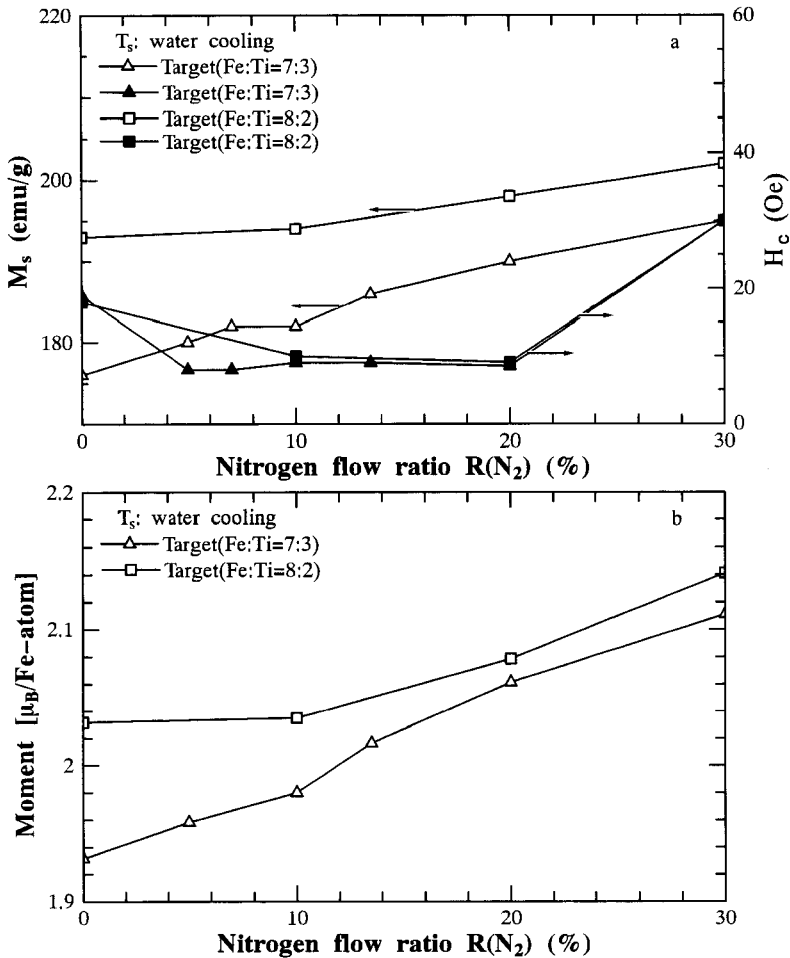
Fig. 10. Variation of a) saturation magnetization M_s and coercivity H_c and b) magnetic moment per Fe atom of the Fe–Ti–N films deposited on water cooled substrates as a function of $R(N_2)$

tion of γ'-Fe$_4$N, being consistent with XRD patterns in Fig. 8. However, it is difficult to understand the change in H_c.

Fig. 12 shows the substrate temperature dependence of M_s and H_c for the films deposited at $R(N_2) = 20\%$. The change is not obvious in M_s, while H_c for the film deposited at $T_s = 250\,°C$ is higher than for the others.

Fig. 13 shows the magnetization curves of the Fe–Ti–N films deposited on water cooled substrates at different $R(N_2)$. Compared with the magnetization curve for $R(N_2) = 0\%$, the magnetization curves for $R(N_2) = 10$ and 20% more easily saturate along the in-plane direction, but the magnetization curve of $R(N_2) = 30\%$ more hardly saturates than that of $R(N_2) = 0\%$. The perpendicular magnetic anisotropy is not observed for the Fe–Ti–N films deposited under the present experimental condition, although Tamai et al. [21] have described perpendicular magnetic anisotropy of Fe–Ti films deposited by rf magnetron sputtering.
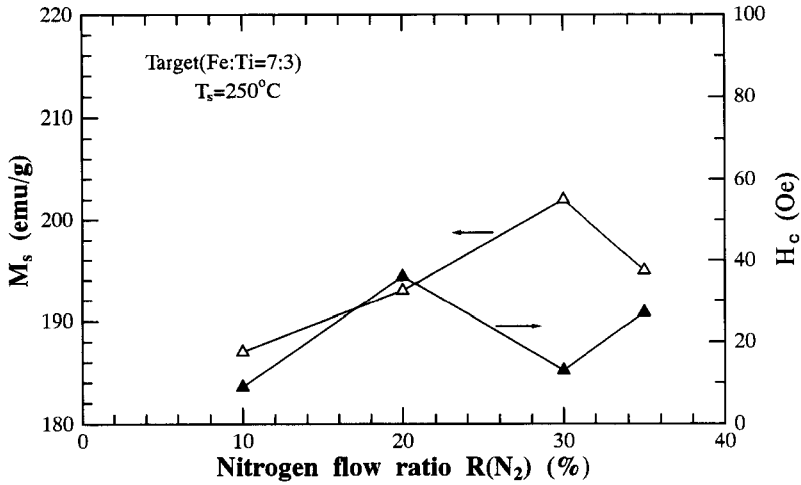
Fig. 11. The saturation magnetization M_s and coercivitiy H_c of the films deposited at $T_s = 250\,^{\circ}\text{C}$ as a function of $R(\text{N}_2)$

4. Conclusion

The structure and magnetic properties of the Fe–Ti–N films prepared by reactive dc magnetron sputtering from composite-type facing targets in an $\text{Ar} + \text{N}_2$ mixture have been investigated. The structure and magnetic properties of the films are sensitive to the nitrogen flow ratio. The incorporation of N into Fe–Ti films suppresses the growth of the α-Fe(110) texture and expands the lattice. For higher nitrogen flow ratios, the TiN_x phase is generated in the Fe–Ti–N films. Comparing with the Fe–N films, the doping of Ti causes a different H_c behavior and suppresses the formation of iron nitride phases.
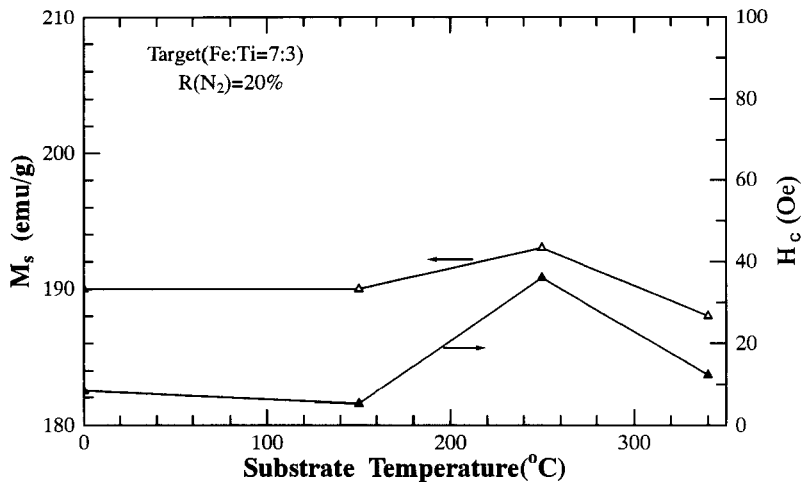
Fig. 12. The saturation magnetization M_s and coercivity H_c of the films deposited at $R(\text{N}_2) = 20\%$ as a function of substrate temperature
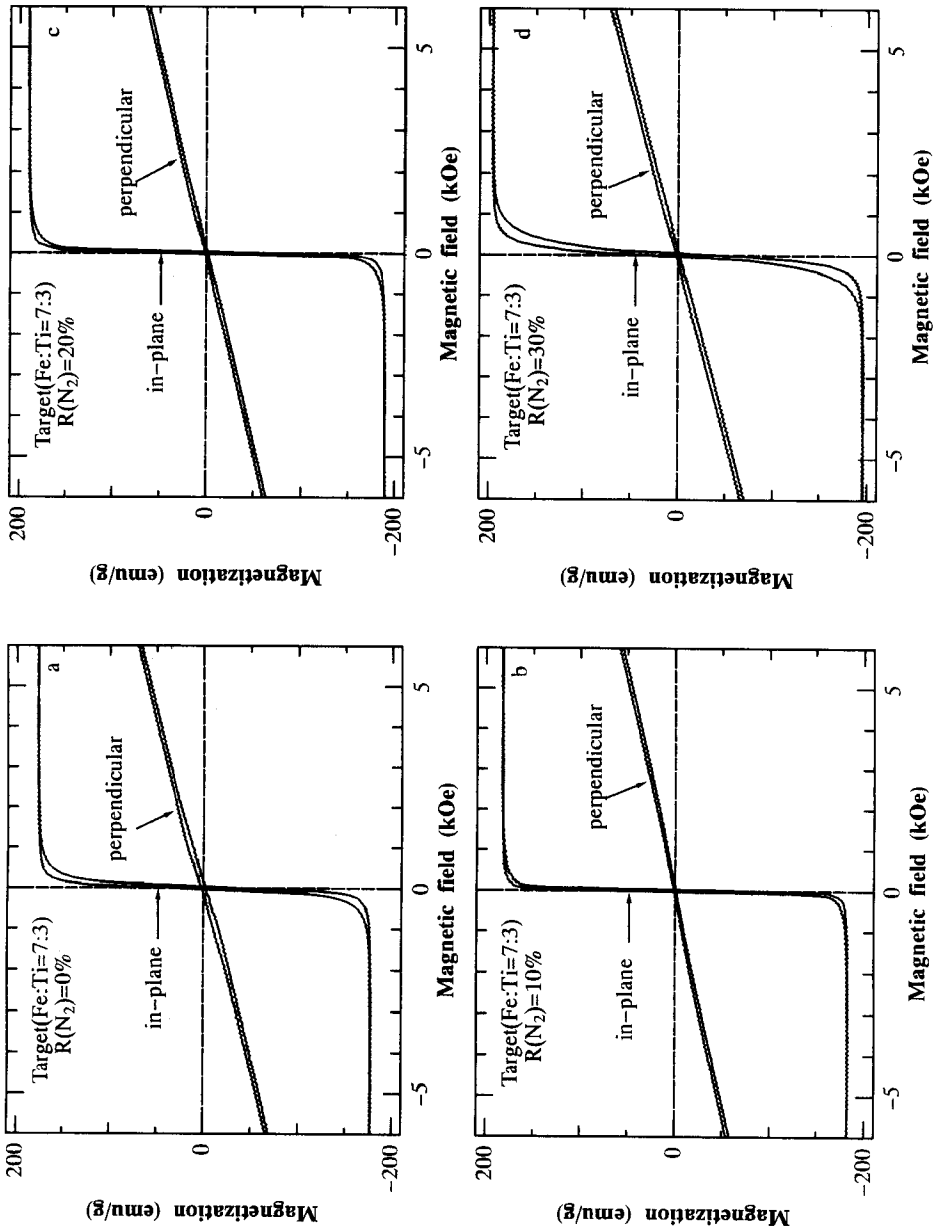
Fig. 13. Magnetization curves at room temperature in magnetic fields parallel and perpendicular to the film planes for the films deposited on water cooled substrates at a) $R(N_2) = 0$, b) 10, c) 20, and d) 30%

References

[1] M. KOMUTO, Y. KOZONO, M. HANAZONO, and Y. SUGITA, J. appl. Phys. **67**, 5126 (1990).

[2] K. NAKAJIMA and S. OKAMOTO, J. appl. Phys. **65**, 4357 (1989).

[3] K. NAKAJIMA and S. MATSUMOTO, Appl. Phys. Letters **56**, 92 (1990).

[4] S. WANG and M. H. KRYDER, J. appl. Phys. **67**, 5134 (1990).

[5] A. MORISAKO, M. MATSUMOTO, and M. NAOE, J. appl. Phys. **69**, 5619 (1991).

[6] H. JIANG, K. TAO, and H. D. LI, J. appl. Phys. **78**, 3299 (1995).

[7] H. JIANG, K. TAO, and H. D. LI, J. Magnetism magnetic Mater. **149**, 358 (1995).

[8] N. ISHIWATA, C. WAKABAYASHI, and H. URAI, J. appl. Phys. **69**, 5616 (1991).

[9] K. NAKANISHI, O. SHIMIZU, and S. YOSHIDA, IEEE Transl. J. Magn. Soc. Japan **15**, 371 (1991).

[10] K. NAGO, H. SAKAKIMA, and K. IHARA, J. Magn. Soc. Japan **7**, 119 (1991).

[11] J. C. LIN, L. J. CHEN, and C. J. CHEN, J. Magn. Soc. Japan **15**, 365 (1991).

[12] G. QIU, E. HAFTEK, and J. A. BARNARD, J. appl. Phys. **73**, 6573 (1993).

[13] K. SUMIYAMA, Y. HASHIMOTO. and Y. NAKAMURA, Trans. Japan. Inst. Metals **24**, 61, 66 (1983).

[14] K. SUMIYAMA, H. EZAWA, and Y. NAKAMURA, phys. stat. sol. (a) **93**, 81 (1986).

[15] K. SUMIYAMA, H. EZAWA, and Y. NAKAMURA, Acta metall. **35**, 1221 (1987).

[16] H. YASUDA, K. SUMIYAMA, and Y. NAKAMURA, J. Phys.: Condensed Mater. **2**, 3595, 9967 (1990).

[17] H. YASUDA, K. SUMIYAMA, Y. NAKAMURA, T. TANAKA, and S. YOSHIDA, phys. stat. sol. (a) **129**, 59 (1992).

[18] J. F. MOULDER, W. F. STICKLE, P. E. SOBOL, and K. D. BOMBEN, in: Handbook of X-Ray Photoelectron Spectroscopy, Ed. J. CHASTAIN, Perkin-Elmer Co., Physical Electronics Division, Minnesota 1992.

[19] C. GAO, W. DOYLE, and M. SHAMSUZZOHA, J. appl. Phys. **73**, 6547 (1993).

[20] M. TAKAHASHI and T. SHIMATSU, J. Magnetism magnetic Mater. **101**, 11 (1991).

[21] H. TAMAI and K. TAGAMI, IEEE Trans. Magnetics **23**, 2737 (1987).